Enhanced Removal of Pb from Electrolytic Manganese Anode Slime by Vacuum Carbothermal Reduction

Yong Yang
cq
Jiancheng Shu (sjcees@126.com)
SWUST
Pengxin Su
SWUST: Southwest University of Science and Technology
Haiping Wu
SWUST: Southwest University of Science and Technology
Lei Zhang
cq
Renlong Liu
cq
Zuohua Liu
cq
Mengjun Chen
swust

Research Article

Keywords: Electrolytic manganese anode slime, vacuum carbothermal reduction method, Pd removal, Chemical MnO2, Resource treatment

Posted Date: November 10th, 2021

DOI: https://doi.org/10.21203/rs.3.rs-990487/v1

Abstract

Electrolytic manganese anode slime (EMAS) is produced during the production of electrolytic manganese metal. In this study, a method based on vacuum carbothermal reduction was used for Pb removal in EMAS. A Pb-removal efficiency of 99.85% and MnO purity in EMAS of 97.34 wt.% was obtained for a reduction temperature of 950°C and a carbon mass ratio of 10% for a holding time of 100 min. The dense structure of the EMAS was destroyed, a large number of multidimensional pores and cracks were formed, and the Pd-containing compound was reduced to elemental Pb by the vacuum carbothermal reduction. A recovery efficiency for chemical MnO_2 of 36.6% was obtained via preparation from Pd-removed EMAS through the “roasting-pickling disproportionation” process, with an acid washing time of 100 min, acid washing temperature of 70°C, H_2SO_4 concentration of 0.8 mol/L, liquid-solid mass ratio of 7 mL/g, calcination temperature of 60°C and calcination time of 2.5 h. Moreover, the crystal form of the prepared chemical MnO_2 was found to be basically the same as that of electrolytic MnO_2, and its specific surface area, micropore volume and discharge capacity were all higher than that of electrolytic MnO_2. This study provides a new method for Pd removal and recycling for EMAS.

Highlights

- Vacuum carbothermal reduction method was used for Pb removal in EMAS.
- The removal efficiency of Pb was 99.85%.
- Chemical MnO_2 with excellent discharge performance was prepared using treated EMAS.
- This study provides a new method for EMAS resource utilization.

1. Introduction

Electrolytic manganese metal (EMM) is an important raw material for industrial production that is widely used in various industrial fields and occupies an important position in the national economy (Zhang et al., 2020). China is a major producer of electrolytic manganese metal (Shu et al., 2019). In 2020, 96.5% of the world's electrolytic manganese metal was produced in China. The production process for EMM mainly includes leaching, impurity removal, electrolysis, and product posttreatment (Tao et al., 2018). Electrolytic manganese anode slime (EMAS) is a solid waste found in the anode chamber during the production of electrolytic manganese metal (Tran et al., 2020). At present, the global annual output of EMM is approximately 1.5 million tons, and approximately 75,000 to 225,000 tons of EMAS is generated each year. In China, most EMAS is dumped as hazardous waste or sold for small additional value. Therefore, EMAS has become a bottleneck hindering the development of the electrolytic manganese industry.

Many scholars have proposed the method of resource-based treatment of EMAS, but the main methods are reduction leaching and acid leaching roasting activation (Zhang et al., 2018). For example, Guo et al. used the roasting leaching method to remove Pd from EMAS and then prepared lithium manganate material from Pd-removed EMAS (Guo et al, 2018). However, the process for this method is more complicated, and the removal efficiency of Pd is low (Chen et al, 2019). Many researchers recycle manganese and Pd from EMAS

by the use of different reducing agents (Chen et al., 2018; Cheng et al., 2009; Li et al., 2017; Niu et al., 2012; Gui et al., 2014; Wei et al., 2017). However, these methods have certain limitations, such as high energy consumption, complex operation, low efficiency and added value (Cheng et al., 2009; Ye et al., 2015; Xie et al., 2021). The removal of Pd and the regulation of the crystal form of manganese oxides are the key factors limiting the application of the above techniques. Regulation of the manganese oxide crystal form and Pb removal have become urgent problems to be solved in the electrolytic manganese metal industry.

The vacuum carbothermal reduction method has always been a research hotspot in the field of vacuum metallurgy, and great research progress has been made (Zhang et al., 2019). The vacuum carbothermal reduction method has the characteristics of both reduction roasting and vacuum smelting and has the characteristics of low energy consumption, simple processing, and environmental friendliness; it is widely used in the fields of chemical engineering and metallurgy (Brkic et al., 2017; Lv et al., 2019; Tian et al., 2020; Xu et al., 2021). Recovery of Pd in the form of pure metallic Pd with a purity of 99.3% from CRT funnel glass by the vacuum carbothermal reduction method has been reported(Qi et al., 2019). Ji et al. and Tang et al. used the vacuum carbothermal reduction method to recover Ga from yellow phosphorus fume and Si from diamond wire-saw silicon powder (Ji et al., 2021; Yang et al., 2019). Tang et al. studied the vacuum carbothermal reduction method to recover lithium and cobalt in waste lithium-ion batteries. The recovery efficiency for Co reaches over 93%, and the recovery efficiency for Li reaches 99% (Tang et al., 2019).

EMAS mainly consists of Mn (52.25 wt.%.), and its phase mainly consists of γ-MnO_2, β-MnO_2 and ε-MnO_2. MnOOH, $PbSO_4$ and $Pb_{2-x}Mn_6O_8$. Pb (6.22 wt.%) and other impurities exist in EMAS, which is disadvantageous to manganese dioxide discharge. It is necessary to control the crystal form of manganese oxide to improve the resource utilization for EMAS (Shu et al., 2017). Manganese oxide undergoes a phase change during the heat treatment process as follows: amorphous manganese oxide is transformed into β-MnO_2 when the temperature is 286.8°C (Liu et al., 2012). MnO_2 is reduced to Mn_2O_3 at 577.3°C, and the content of Mn_2O_3 increases with increasing temperature. Mn_2O_3 is then reduced to Mn_3O_4 at a temperature of 761.3°C (Jacob et al., 2011).

In this study, the vacuum carbothermal reduction method was first used for Pb-removal in EMAS. The effects of process parameters such as reduction temperature, holding time and mass ratio of carbon on the Pd-removal process were investigated, and the removal mechanism for Pd was analyzed. In addition, the preparation process for chemical MnO_2 by the “roasting-acid washing disproportionation” process was studied. This study provided a new idea for the high-value resource utilization of EMAS.

2. Materials And Methods

2.1 Raw material

The EMAS samples used in this paper were all sampled in an electrolytic manganese plant in Chongzuo, Guangxi, according to the "technical specification for sampling and preparation of industrial solid waste". The EMAS samples were dried at 80°C, milled by ball milling and screened through 200 mesh for standby.

H_2SO_4 and other chemical reagents were analytically pure and purchased from Chongqing Boyi Chemical Reagent Co., Ltd.

2.2 Experiment for Pd removal

First, the EMAS was pretreated by washing and drying. Secondly, a certain mass of pretreated EMAS and a certain mass ratio of activated carbon (4 wt%, 6 wt%, 8 wt%, 10 wt%, 12 wt%) were transferred to an agate mortar for full mixing. Finally, the sample boat was placed into the middle of a tubular furnace, and the vacuum pump and tubular furnace were started. The sample was then roasted at a set reaction temperature (850°C, 900°C, 950°C, 1000°C and 1050°C), held for a certain time (70 min, 80 min, 90 min, 100 min and 110 min), and then naturally cooled to room temperature.

2.3 Preparation of chemical MnO_2

Chemical MnO_2 was prepared from Pb-removed EMAS by a “roasting-acid washing disproportionation” process. The roasting process is the key step affecting the preparation of chemical MnO_2 from Pd-removed EMAS (MnO), while the acid washing process has little effect on the conversion efficiency of chemical MnO_2 (Ye et al. 2017). Therefore, the effects of calcination temperature (450°C, 500°C, 550°C, 600°C, 650°C) and calcination time (1.5 h, 2 h, 2.5 h, 3 h, 3.5 h) on the conversion of chemical MnO_2 were investigated. The process parameters used for acid washing disproportionation were as follows: acid washing time of 100 min, acid washing temperature of 70°C, H_2SO_4 concentration of 0.8 mol/L, and liquid-solid mass ratio of 7 mL/g.

2.4 Discharge performance test for chemical MnO_2

The prepared sample electrode (0.032 g sample) was used as the working electrode, a zinc sheet (1 cm×1 cm) was used as the reference electrode and counter electrode, and a 9 mol/L KOH saturated solution was used as the electrolyte. The constant current discharge method was used to measure the specific capacity of the sample, and the termination voltage was 1.0 V. The specific capacity was determined using the calculation method shown in equation 1:

$$C = \frac{IT}{m} \quad (1)$$

Where C ($mAh \cdot g^{-1}$) is the specific capacity of the sample to be tested; I (mA) is the discharge current; T (h) is the discharge time; and m (g) is the mass of the sample.

2.5 Analysis method

X-ray fluorescence (XRF) (XRF-1800, Japan) was used to analyze the elemental composition of the EMAS sample. X-ray diffraction (XRD) (D/Max-2500, Japan) and scanning electron microscopy (SEM) (JSM-7800F, Japan) were used to analyze the phase composition and microstructure of EMAS and EMAS after vacuum carbothermal reduction and chemical MnO_2. The specific surface area and pore diameter of chemical MnO_2 were analyzed by the Brunauer-Emmett-Teller (BET) method (3H-2000PS1, Best Instrument

Technology Co., Ltd., China.). The discharge performance of electrolytic MnO_2 and chemical MnO_2 was analyzed by using an electrochemical workstation (CHI660E, Shanghai Chen hua Instrument Co., Ltd., China.). The Pb content was determined by XRF, and the following formula was used to calculate the Pb-removal efficiency:

$$\varphi_{\mathrm{Pb}}=\frac{\mathrm{C}_0-\mathrm{C}_\mathrm{e}}{\mathrm{C}_0}\times 100\% \quad (2)$$

$$\varphi_{\mathrm{Mn}}=\frac{\mathrm{m}_0-\mathrm{m}_\mathrm{e}}{\mathrm{m}_0}\times 100\% \quad (3)$$

Where φ_{Pb} (%) is the removal efficiency for Pb; C_0 ($mg \cdot g^{-1}$) is the original Pb content; C_e ($mg \cdot g^{-1}$) is the Pb content after vacuum carbothermal reduction treatment; φ_{Mn} (%) is the conversion efficiency for chemical MnO_2; m_0 ($mg \cdot g^{-1}$) is the original weight of Mn in EMAS after vacuum carbothermal reduction treatment; and m_e ($mg \cdot g^{-1}$) is the weight of Mn in MnO_2 after “roasting - acid washing disproportionation” treatment.

3. Results And Discussion

3.1 Removal behavior for Pd

The Pb-removal efficiency in EMAS increased with increasing reduction temperature (Fig. 1a). The Pd-removal efficiency was 85.12% and 99.85% when the reduction temperature was 850°C and 950°C, respectively. Then, the reduction temperature continued to increase, and although the Pb-removal efficiency increased slightly, this increase was not obvious. Therefore, considering the energy consumption, the reduction temperature was suggested to be 950°C. As shown in Fig. 1b, within the time range selected in the experiment, the removal efficiency for Pb in EMAS increased obviously with time, but when the holding time exceeded 100 min, the change in the Pb-removal efficiency was small, so it was better to select a holding time of 100 min. When the carbon mass ratio reached 10%, the Pb-removal efficiency basically tended to be stable, which changed from 99.85–99.88% (Fig. 1c). This can be explained by the fact that the amount of reducing agent was not enough to fully reduce the Pb compounds in the EMAS when the proportion of carbon was relatively small, which led to a poor removal effect for Pb. When the proportion of activated carbon reached 10%, the Pb compounds in the EMAS were fully reduced, so it was better to choose the proportion of carbon as 10%. The optimum Pb-removal efficiency was 99.85%.

3.2 Removal Mechanism for Pd

In Table 1 and Table 2, the MnO content was 97.34 wt. %, and the Pb content was decreased from 6.22 wt. % to 0.01 wt. %. These results indicate that vacuum carbothermal reduction can be used for Pb removal in EMAS. As shown in Fig. 2a, the XRD characteristic spectrum for EMAS is relatively disordered, which indicates that the crystallinity of various phases contained in EMAS is low. The XRD characteristic peaks for

EMAS are mainly divided into two categories, namely, high valence oxides of Mn and Pb compounds. Specifically, EMAS contains three different crystal forms: MnO_2 (γ, β, ε), MnOOH, $MnO_{1.88}$, $MnSO_4$, $(NH_4)_2SO_4$, $PbSO_4$, and $Pb_{2-x}Mn_6O_8$. $MnSO_4$ and $(NH_4)_2SO_4$ mainly arise from the electrolyte. From Fig. 2b, the results show that the EMAS crystallinity was enhanced during the vacuum carbothermal reduction treatment at 450°C, 600°C, 700°C and 950°C. The hydroxides of $Mn(OH)_4$ and other high valence manganese were dehydrated to MnO_2, MnO_2 was finally reduced to Mn_3O_4, and $PbSO_4$ and PbO_2 in EMAS were reduced to PbO. MnO was the main phase in EMAS, which indicated that MnO_2 was completely reduced to MnO when the temperature ranged between 700°C and 950°C. All Pd compounds in EMAS were reduced to Pd when the temperature was higher than 700°C. The main phase was MnO with good crystallinity and no impurity peak observed when the temperature was 950°C, which indicated that Pb was almost completely removed from EMAS. As shown in Fig. 2c, the black condensate collected in the vacuum tubular furnace was metallic Pb, which further proved that the Pb-containing compounds in the EMAS were removed by Pd vapor.

Table 1. Chemical composition of electrolytic manganese anode slime

Element	Mn	Pb	Se	Fe	O	S	Ca	Sn	Si	Al	Others
Content/wt.%	52.25	6.22	0.27	0.46	32.72	2.47	0.79	0.15	0.12	0.01	4.54

Table 2. Chemical composition of electrolytic manganese anode slime after Pd removal (temperature 950 °C, holding time 100 min and carbon mass ratio 10%)

Element	Mn	O	Ca	Fe	S	Si	Al	others
Content/wt.%	75.18	22.16	0.98	0.56	0.75	0.23	0.01	0.11

As shown in Fig. 3a, SEM for the raw EMAS particles presented a relatively dense state. As shown in Fig. 3b to Fig. 3d, the dense structure of the EMAS main body was gradually destroyed, and a large number of multidimensional pores and cracks were formed as the temperature was increased. These multidimensional pores and cracks were formed due to the loss of O atoms in the crystal of the main phase of EMAS (MnO_2) during the vacuum carbothermal reduction treatment, and the local grain size was greatly reduced (Zhang et al., 2016). These multidimensional pores and cracks provided channels for the volatilization and removal of Pb metal generated in the vacuum carbothermal reduction process for EMAS (Ye et al., 2017). The above results show that Pb can be feasibly removed in EMAS under high temperature and vacuum conditions.

Based on XRF, XRD, SEM and thermodynamic analysis (thermodynamic analysis of the behavior of Pd is shown in the supporting information), the possible reaction of MnO_2 and Pb during the vacuum carbothermic reduction process is expressed as follows:

1. Reduction reactions for MnO_2:

$2MnO_2 + C = Mn_2O_3 + CO$ (g) (4)

$3Mn_2O_3 + C = 2\ Mn_3O_4 + CO$ (g) (5)

$Mn_3O_4 + C = 3\ MnO + CO$ (g) (6)

$2MnO_2 + CO = Mn_2O_3 + CO_2$ (g) (7)

$3Mn_2O_3 + CO = 2\ Mn_3O_4 + CO_2$ (g) (8)

$Mn_3O_4 + CO = 3\ MnO + CO_2$ (g) (9)

$CO_2 + C = 2CO$ (10)

2. Pb-removal reactions:

$2\ PbSO_4 + C = 2\ PbO + 2\ SO_2$ (g)+ CO_2 (g) (11)

$PbSO_4 + CO = PbO + SO_2$ (g)+ CO_2 (g) (12)

2 Pbo + Co = Pbo + Co (G) (13)
$Pb_2O + CO = 2Pb(g) + CO_2$ (g) (14)

$CO_2 + C = 2CO$ (15)

3.3 Preparation of chemical MnO_2

As shown in Fig. 4a and Fig. 4b, the conversion efficiency of chemical MnO_2 (CMD) increased with increasing temperature, increasing from 20.4–37.2%. When the temperature exceeded 600°C, the conversion efficiency for CMD increased slightly. Therefore, it was better to choose a roasting temperature of 600°C at which the conversion efficiency for CMD was 36.6%. When the roasting time was less than 2.5 h, the CMD conversion efficiency increased obviously with time (from 28.3–36.6%); when the roasting time was more than 2.5 h, the CMD conversion efficiency increased slightly (from 36.6–38.5%), and with the increasing calcination time, the economy worsened. Therefore, the optimum roasting time was 2.5 h for a CMD conversion efficiency of 36.6%.

As shown in Fig. 5, the crystal forms of chemical MnO_2 (CMD) and electrolytic MnO_2 (EMD) were basically the same. Compared with the standard card, the main crystal form was γ - MnO_2. There were many lattice defects, no ideal ratio and vacancies in the crystal form of γ - MnO_2, which has the characteristics of a large cross-sectional area of crystal tunnels and high electrochemical activity. This type of crystal form for γ -

MnO_2 is widely used in power batteries and alkaline manganese batteries and other industries, which affords the prepared CMD with natural advantages due to its crystal form and provides a large number of application scenarios for the high-value resource utilization of CMD (Guo et al., 2007; Xiao Chai et al., 1978). As shown in Fig. 6a and Fig. 6b, the CMD particle size was larger than that of EMD, the particles were staggered and stacked together, there was a substantial agglomeration phenomenon, and the particle size of the aggregate was approximately 1 μm.

3.4 Discharge performance of chemical MnO_2

Figure 7a and 7b shows discharge curves for EMD and CMD in 9 mol/L KOH (ZnO saturated) solution with different discharge currents at 1.0 V, respectively. The potential plateau in the discharge curve is attributed to the transformation between manganese dioxide and metal (Chen et al., 2017). The discharge platforms for CMD and EMD were basically the same. The discharge plateau for CMD was more stable and lasted longer at a discharge current of 0.1 A/g, 0.3 A/g and 0.4 A/g. As shown in Fig. 7c, the discharge capacity of CMD was 240.84 mAh/g, and the discharge capacity of EMD was 223.96 mAh/g when the discharge current was 0.1 A/g. The results showed that the discharge performance of CMD was better than that of EMD.

A comparative analysis of CMD and EMD by the BET test is shown in Fig. 8. The adsorption capacity of the prepared CMD was greater than that of EMD. The specific surface area of CMD was 45.2607 $m^2 \cdot g^{-1}$, while that of EMD was only 28.3444 $m^2 \cdot g^{-1}$, which is consistent with the SEM results. According to the IUPAC classification, the adsorption isotherms for CMD and EMD can be classified as type II with H_3-type hysteresis, respectively (Thevenot et al., 1996). In the range of $P/P_0 \leq 0.40$, the N_2 adsorption capacity of CMD and EMD increased gradually with increasing relative pressure, and the adsorption curve and analytical curve overlapped in this region, which indicated a small amount of microporous adsorption and monolayer adsorption (Shu et al., 2017). When P/P0 > 0.40, the adsorption capacity of N_2 increased rapidly, and H_3-type hysteresis was observed at relatively high pressure, which was due to the capillary condensation and multilayer adsorption of N_2 in mesopores and macropores, indicating that the pores in CMD and EMD are narrow slit-like pores (Bakandritsos et al,. 2004; Bu et al., 2010). According to the Dubinin-Radushkevich model, the micropore volume of CMD was 0.0896 $cm^3 \cdot g^{-1}$, while that of EMD was only 0.0489 $cm^3 \cdot g^{-1}$. The average pore size of CMD was 7.92 nm and that of EMD was 6.90 nm. Therefore, it was considered that the specific surface area and pore size of CMD is higher than those for EMD, which may be one of the reasons for the better discharge performance of CMD.

4. Conclusion

In this study, the vacuum carbothermal reduction method was used for Pd-removal from EMAS. In this process, the main phase of EMAS was reduced to MnO, and the Pd-containing compounds were gradually reduced to metal Pd and volatilized. A Pd-removal efficiency of 99.85% and MnO powder purity in EMAS of 97.34% was obtained at a reduction temperature of 950°C, carbon mass ratio of 10%, and holding time of 100 min. A Mn recovery efficiency of 36.6% was obtained by the “roasting-acid washing disproportionation”

process under the following conditions: acid washing time of 100 min, acid washing temperature of 70°C, H_2SO_4 concentration of 0.8 mol/L, liquid-solid mass ratio of 7 mL/g, calcination temperature of 60°C and calcination time of 2.5 h. The crystal form of CMD was basically the same as that of EMD, and the specific surface area and micropore volume of CMD were higher than those of EMD. The discharge capacity of CMD was 16.88 mAh/g, which was higher than that of EMD at a discharge current of 0.1 A/g. This study provides a new method for the recycling of EMAS.

Declarations

Ethics approval and consent to participate

Approval was obtained from the ethics committee of Southwest University of Science and Technology. The procedures used in this study adhere to the tenets of the Declaration of Helsinki.

Consent to Publish

Informed consent was obtained from all individual participants included in the study.

Funding

All sources of funding for the research reported should be declared. The role of the funding body in the design of the study and collection, analysis, and interpretation of data and in writing the manuscript should be declared.

Availability of data and materials

All data generated or analysed during this study are included in this published article (and its supplementary information files).

Acknowledgement

This work was supported by ‘National Natural Science Foundation of China’ (21806132), ‘National Key R&D Program of China’ (2018YFC1903500), ‘Sichuan Province Science and Technology plan-Key Research and Development’ (19ZDYF0911), ‘Science and Technology Plan Project of Sichuan Province (2021YFH0058)’, ‘Science and Technology Program of Guizhou Province-China’ ([2019]2863),‘Science and Technology Project of Mianyang City, Sichuan Province (2019YFZJ014)’,‘Key R & D Program of Guangxi Province’ (AB18126088).

References

1. A. Bakandritsos, T. Steriotis, D. Petridis, 2004. High surface area montmorillonite-carbon composites and derived carbons. Chem. Mater. 16, 1551–1559.
2. Brkic, M., Koepf, E., Meier, A., 2017. Solar carbothermal reduction of aerosolized ZnO particles under vacuum: Modeling, experimentation, and characterization of a drop tube reactor. Chemical Engineering

Journal. 313, 435-449.

3. Bu, X.-Z., Zhang, G.-K., Gao, Y.-Y., Yang, Y.-Q., 2010. Preparation and photocatalytic properties of visible light responsive N-doped TiO2/rectorite composites. Microporous and Mesoporous Materials. 136, 132-137.
4. Chen, X., Zhu, Y., Li, B., Hong, P., Luo, X., Zhong, X., Xing, L., Li, W., 2017. Porous manganese oxide nanocubes enforced by solid electrolyte interphase as anode of high energy density battery. Electrochimica Acta. 224, 251-259.
5. Chen, Y., Liu, N., Ye, L., Xiong, S., Yang, S., 2018. A cleaning process for the removal and stabilisation of arsenic from arsenic-rich lead anode slime. Journal of Cleaner Production. 176, 26-35.
6. Chen Z., Mao Y., 2019. Studies on Rotary Kiln Reduction Roasting Technology for the Treatment of High Valence Insoluble Manganese Ore Resources. metal mine. 09, 78-82.
7. Cheng, Z., Zhu, G., Zhao, Y., 2009. Study in reduction-roast leaching manganese from low-grade manganese dioxide ores using cornstalk as reductant. Hydrometallurgy. 96, 176-179.
8. D.R. Thevenot, K. Toth, R.A. Durst, G.S. Wilson, 1996. International Union of Pure and Applied Chemistry - physical chemistry division, steering committee on biophysical chemistry - analytical chemistry division, commission V.5 (electroanalytical chemistry) - electrochemical biosensors: proposed definitions and classification synopsis of the report, Sensor Actuat B-Chem. 30, 81–84.
9. Guo S., 2018. Purification of electrolytic manganese anode slime and preparation of lithium rich manganese based cathode materials. Wuhan University of Technology.
10. Jacob, K.T., Kumar, A., Rajitha, G., Waseda, Y., 2011. Thermodynamic data for Mn 3 O 4 ,Mn 2 O 3 and MnO 2 . High Temp. Mater. Process 30, 459–472..
11. Ji, W., Xie, K., Huang, H., Chen, H., 2021. Recovery of gallium from yellow phosphorus flue dust by vacuum carbothermal reduction. Journal of Cleaner Production. 284.
12. Li Y., Li X., Ye H., Kong X., 2017. Leaching of Electrolytic Manganese Anode Slimes in SO2-H2SO4-H2O System. Hydiometallurgy of China. 36(06): 473-475.
13. Liu G., Sheng H., Wang Q., 2014. Recovery of manganese and lead from manganese electrowinning anode slime by reduction leaching with organic reductants, Mining and Metallurgigal Engineering 34, 92–98.
14. Liu, J., Li, Z., Liu, Y., Yang, H., Liang, L., 2012. Study on decomposition dynamics of manganese dioxide. Trans. Nonferrous Met. Soc. China 12, 8–12.
15. Lv, X., Huang, R., Wu, Q., Xu, B., Zhang, J., 2019. Non-isothermal reduction kinetics during vacuum carbothermal reduction of ilmenite concentrate. Vacuum. 160, 139-145.
16. Niu S., Wang Z., Guo H., Li H., Peng W., Hu Q., Zhang Y., 2012. Reductive leaching of manganese from manganese anode slag. The Chinese Journal of Nonferrous Metals. 22(09): 2662-2666.
17. Qi, Y., Xiao, X., Lu, Y., Shu, J., Wang, J., Chen, M., 2019. Cathode ray tubes glass recycling: A review. Science of The Total Environment. 650, 2842-2849.
18. Shu, J., Liu, R., Liu, Z., Wu, H., Chen, Y., Tao, C., 2017. Enhanced discharge performance of electrolytic manganese anode slime using calcination and pickling approach. Journal of Electroanalytical

Chemistry. 806, 15-21.

19. Shu, J., Wu, H., Chen, M., Peng, H., Li, B., Liu, R., Liu, Z., Wang, B., Huang, T., Hu, Z., 2019. Fractional removal of manganese and ammonia nitrogen from electrolytic metal manganese residue leachate using carbonate and struvite precipitation. Water Research. 153, 229-238.
20. Tang, Y., Xie, H., Zhang, B., Chen, X., Zhao, Z., Qu, J., Xing, P., Yin, H., 2019. Recovery and regeneration of LiCoO2-based spent lithium-ion batteries by a carbothermic reduction vacuum pyrolysis approach: Controlling the recovery of CoO or Co. Waste Management. 97, 140-148.
21. Tao C., Liu Z., Fan X., 2018. Energy saving and emission reduction theory and engineering application of electrolytic manganese.
22. Tian, Y., Wang, L., Yang, B., Dai, Y., Xu, B., Wang, F., Xiong, N., 2020. Comparative evaluation of energy and resource consumption for vacuum carbothermal reduction and Pidgeon process used in magnesium production. Journal of Magnesium and Alloys.
23. Tran, C. C. H., Santos-Pena, J., Damas, C., 2020. Electrodeposited manganese oxide supercapacitor microelectrodes with enhanced performance in neutral aqueous electrolyte. Electrochimica Acta. 335.
24. Wei H., Yang Y., Luo D., Wu X., Lu Q., Huang H., 2017. A Research on Comprehensive Recycling of Electrolytic Manganese Anode Slime. China's Manganese Industry. 35(S1): 55-58.
25. Xie, H., Li, S., Guo, Z., Xu, Z., 2021. Extraction of lead from electrolytic manganese anode mud by microwave coupled ultrasound technology. Journal of hazardous materials. 407, 124622-124622.
26. Xiao Chai C., Xi Ze M., 1978. Crystal structure and chemical composition of electrolytic manganese dioxide. Battery Bimonthly. (02): 40-46.
27. Xu, Y., Zhou, Z., Chen, X., Han, C., Yang, B., Xu, B., Liu, D., 2021. Ultrafine AlN synthesis by alumina carbothermal reduction under vacuum: Mechanism and experimental study. Powder Technology. 377, 843-846.
28. Yang, S., Ma, W., Wei, K., Xie, K., Wang, Z., 2019. Thermodynamic analysis and experimental verification for silicon recovery from the diamond wire saw silicon powder by vacuum carbothermal reduction. Separation and Purification Technology. 228.
29. Ye, L., Tang, C., Chen, Y., Yang, S., Yang, J., Zhang, W., 2015. One-step extraction of antimony from low-grade stibnite in Sodium Carbonate - Sodium Chloride binary molten salt. Journal of Cleaner Production. 93, 134-139.
30. Ye Q., 2017. Microwave enhanced carbothermal reduction of low grade pyrolusite. Kunming University of science and technology.
31. Zhang, C., Jiang, L., Xu, F., Duan, N., Xin, B., Han, G., Zhang, G., Wen, Y., 2018. New insight into cleaner control of heavy metal anode slime from aqueous sulfate electrolytes containing Mn (II): Preliminary characterization and mechanism analysis. Journal of Cleaner Production. 177, 276-283.
32. Zhang, H., Bi, Y., Chen, X., Huang, L., Mu, L., 2016. Treatment and Characterization Analysis of Electrolytic Manganese Anode Slime. Procedia Environmental Sciences. 31, 683-690.
33. Zhang, R., Ma, X., Shen, X., Zhai, Y., Zhang, T., Ji, C., Hong, J., 2020. Life cycle assessment of electrolytic manganese metal production. Journal of Cleaner Production. 253, 119951.

34. Zhang Y., Lin H., Gu C., 2019. Technical analysis of vacuum metallurgy of nonferrous metals. Metallurgy and Materials. 39(05): 174+176.

Supporting Information

Supporting Information is not available with this version.

Figures

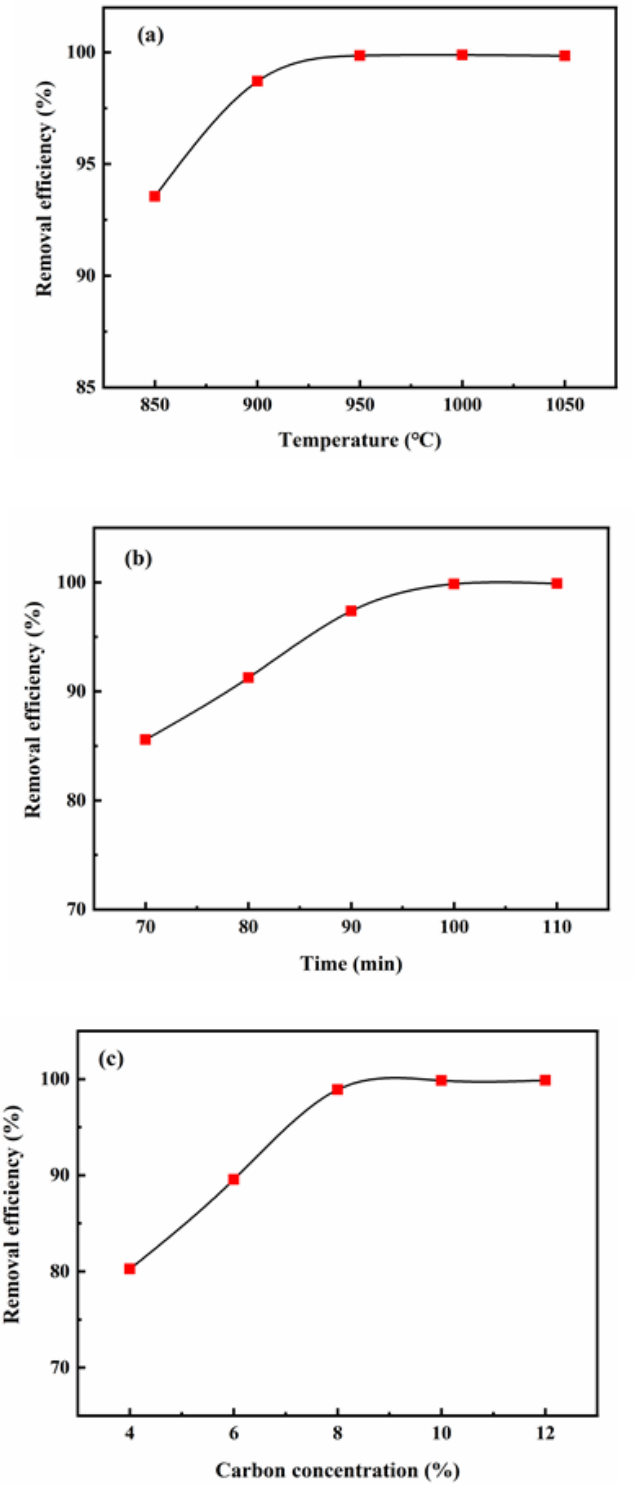

Figure 1

Effect of reduction temperature (a, carbon mass ratio 10%, holding time 100 min); time (b, carbon mass ratio 10%, reduction temperature 950 °C); carbon mass ratio (reduction temperature 950 °C, holding time 100 min) on Pd-removal efficiency

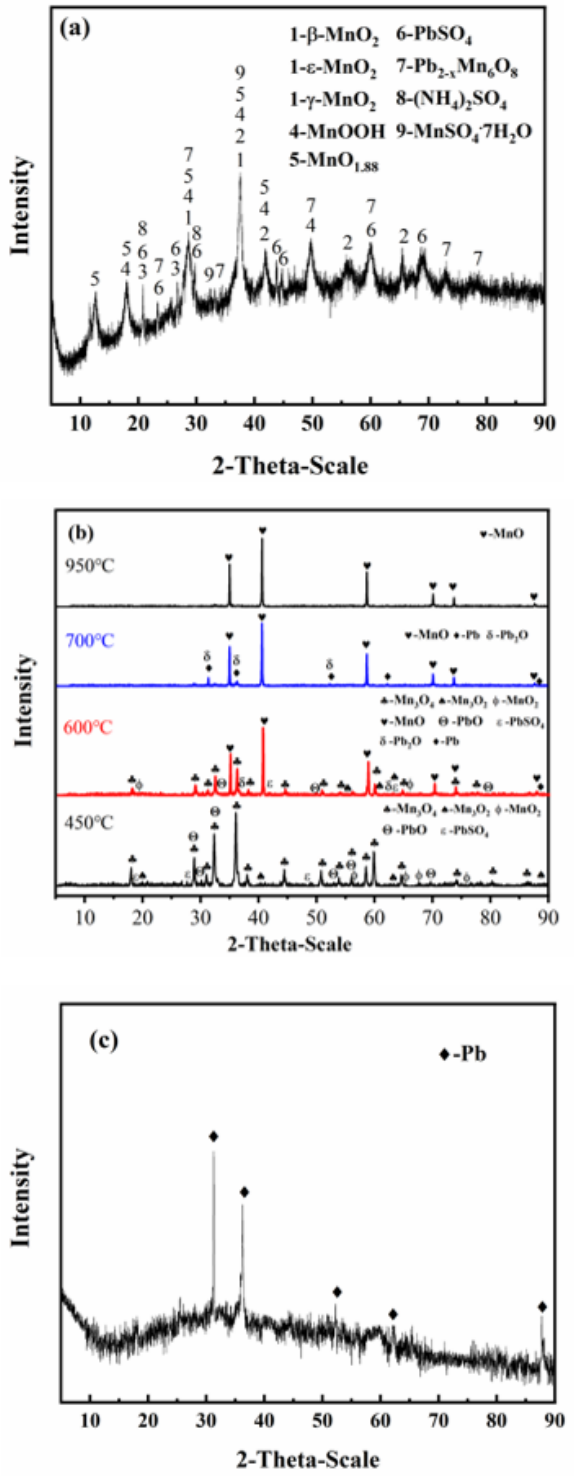

Figure 2

XRD pattern for the initial EMAS (a), EMAS after treatment at different temperatures of 450°C (b), XRD pattern for the black condensate collected in the vacuum tubular furnace (c).

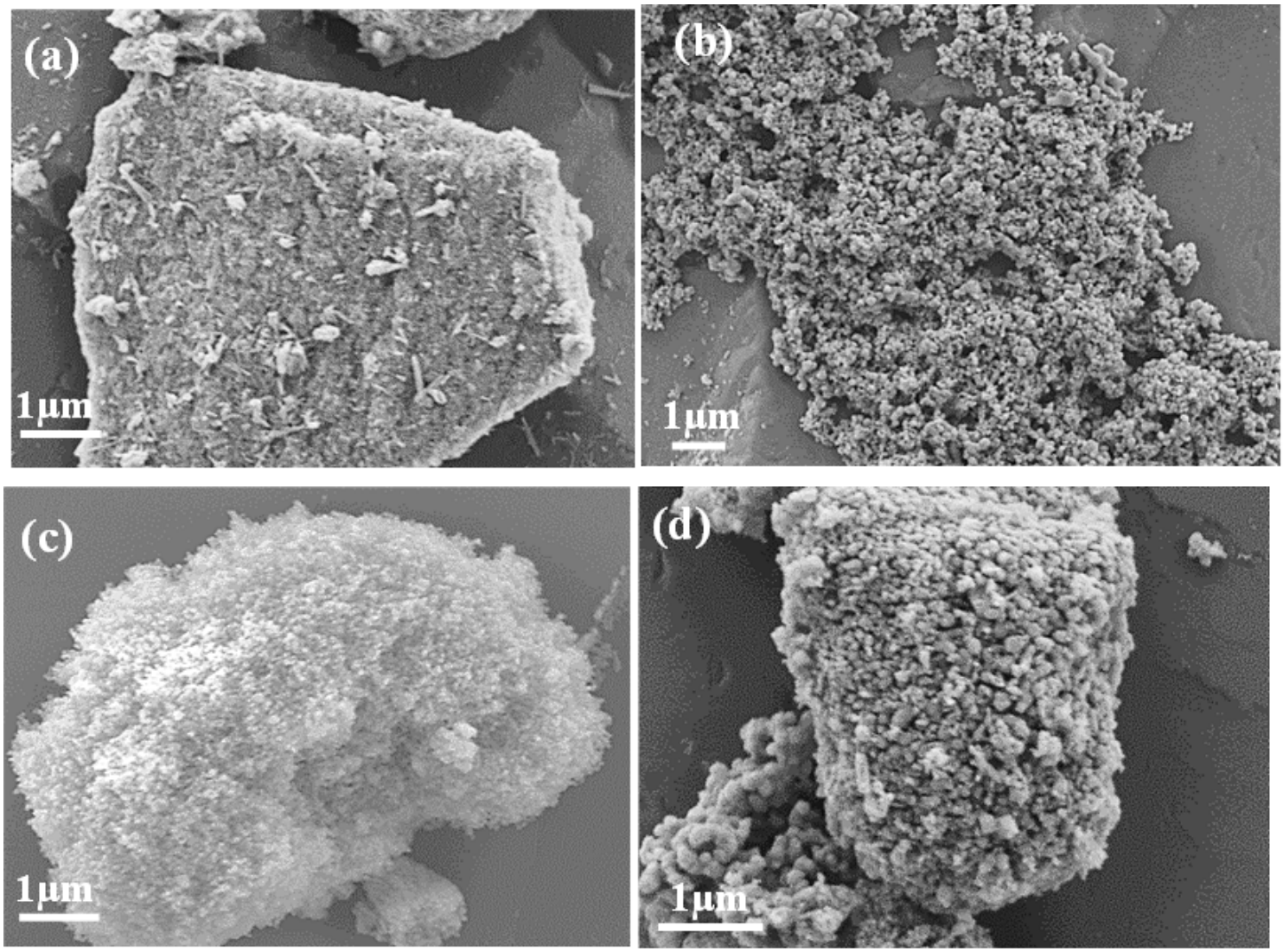

Figure 3

SEM micrographs for EMAS after treatment at different temperatures. Initial EMAS (a); 450 °C (b); 600 °C (c); 700 °C (d)

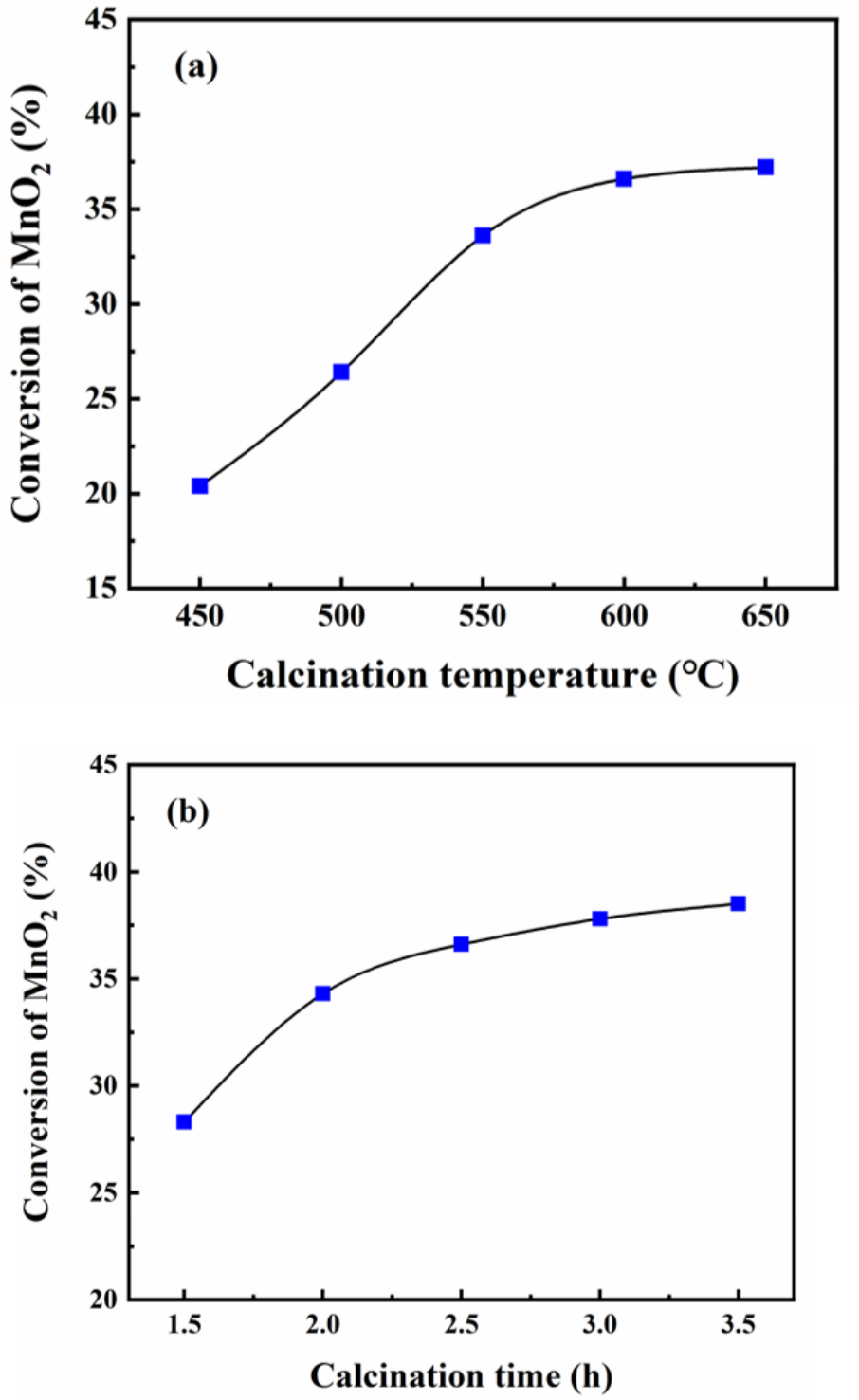

Figure 4

Effect of calcination temperature on CMD conversion efficiency with calcination temperature as 2 h (a) and effect of calcination time on CMD conversion efficiency with a calcination temperature of 600 °C (b)

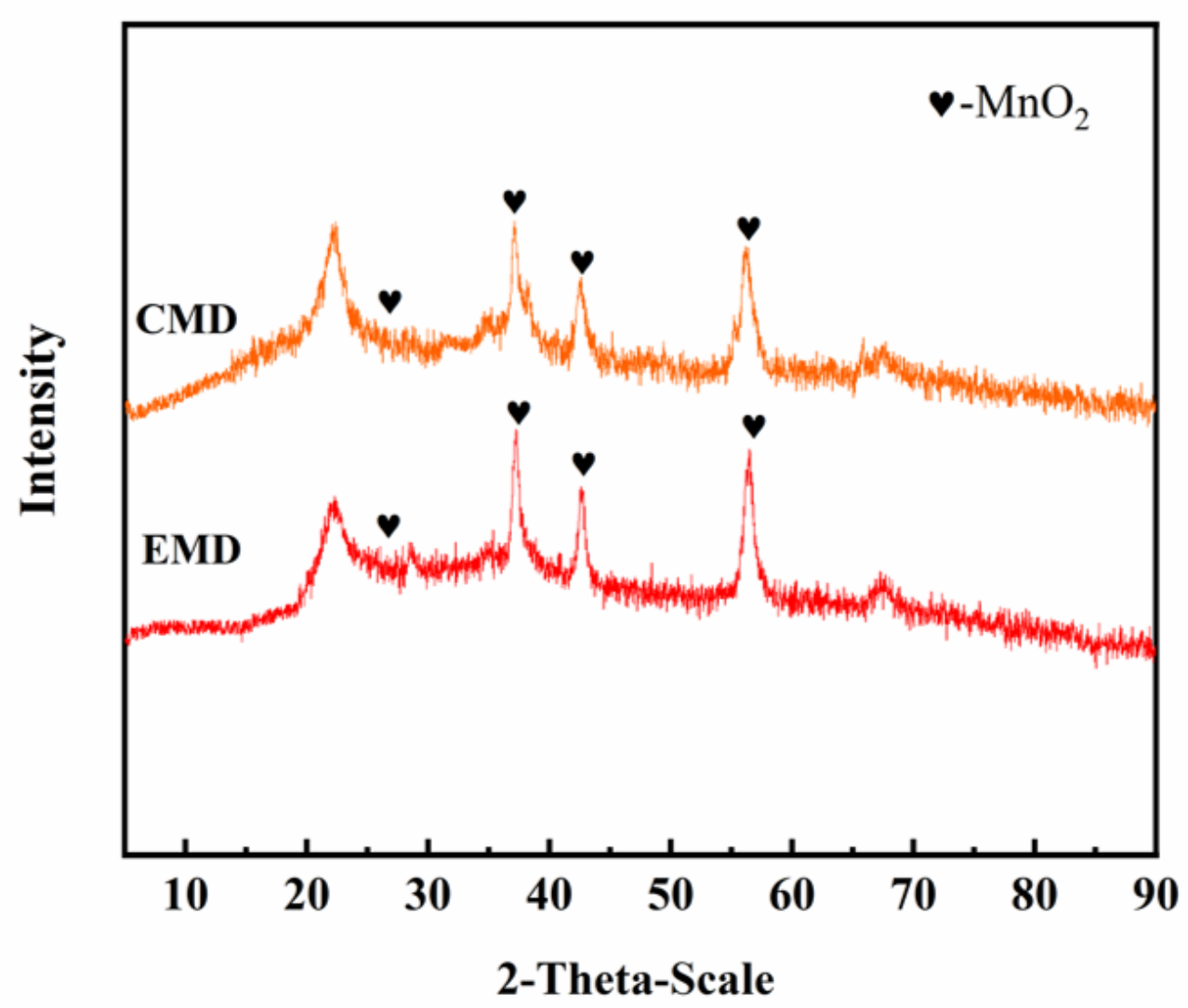

Figure 5

XRD patterns for CMD and EMD

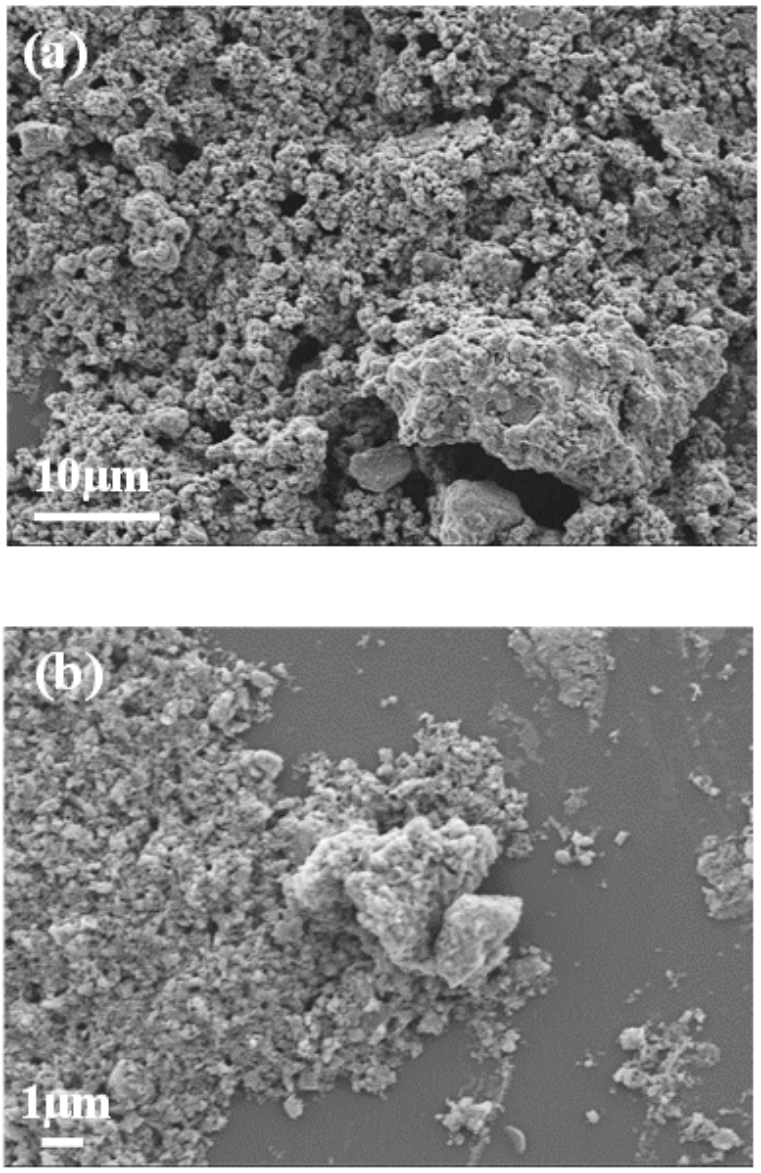

Figure 6

SEM paragraphs of CMD (a) and EMD (b)

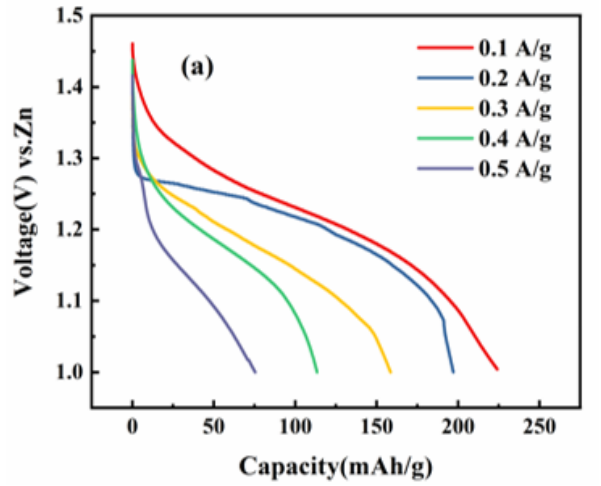

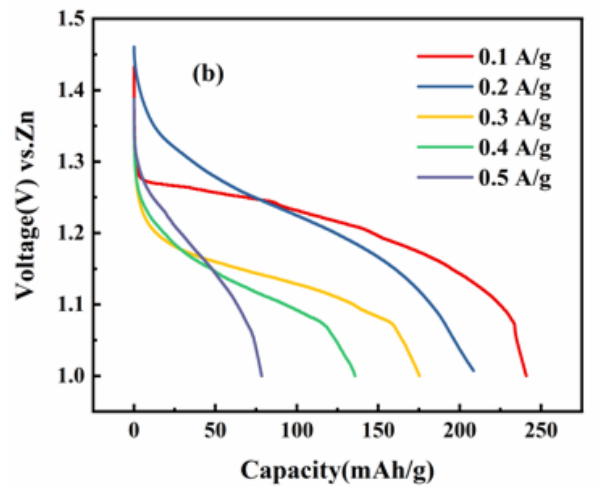

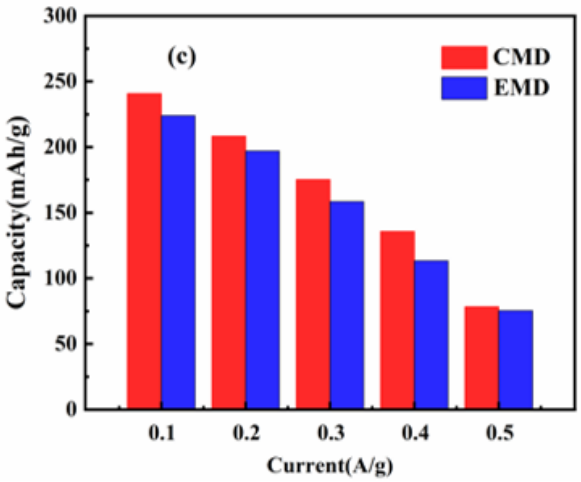

Figure 7

Constant current curve EMD (a), CMD (b) and discharge capacity comparison diagram for CMD-EMD (c)

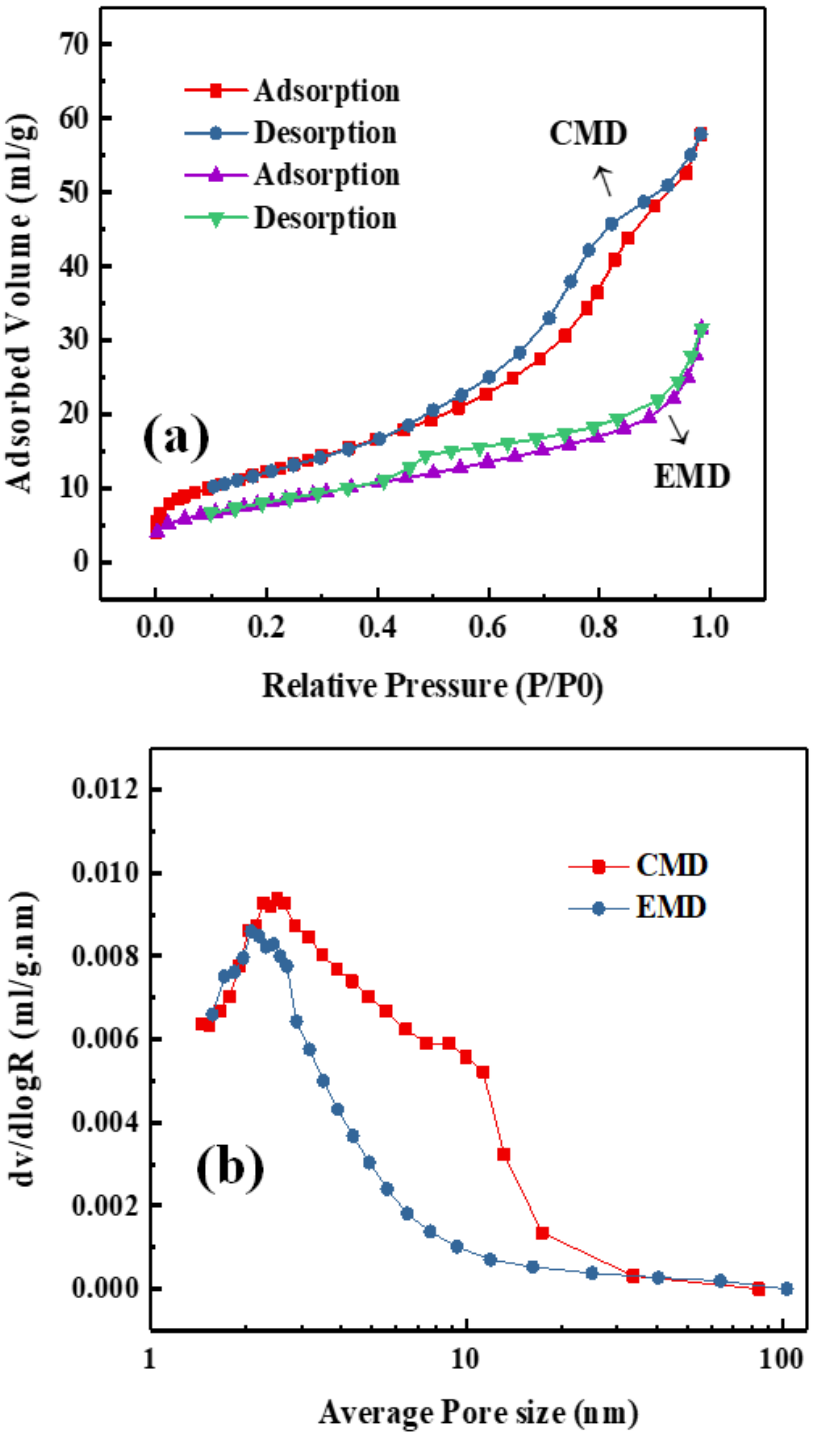

Figure 8

N2 adsorption-desorption isotherms for CMD and EMD (a), Pore size distributions for CMD and EMD (b)

Supplementary Files

This is a list of supplementary files associated with this preprint. Click to download.

- GA.png